Journal of Scientific Computing (© 2005)
DOI: 10.1007/s10915-005-9000-9

CFL-Violating Numerical Schemes for a Two-Fluid Model

Steinar Evje[1] **and Tore Flåtten**[1,2]

Received October 4, 2004; accepted (in revised form) June 13, 2005

In this paper we propose a class of linearly implicit numerical schemes for a two-phase flow model, allowing for violation of the CFL-criterion for all waves. Based on the *Weakly Implixit Mixture Flux* (WIMF) approach [SIAM J. Sci. Comput., 26 (2005), pp. 1449–1484], we here develop an extension denoted as *Strongly Implicit Mixture Flux* (SIMF).

Whereas the WIMF schemes are restricted by a weak CFL condition which relates time steps to the fluid velocity, the SIMF schemes are able to break the CFL conditions corresponding to both the sonic and advective velocities.

The schemes possess some desirable features compared to current industrial pressure-based codes. They allow for sequential updating of the momentum and mass variables on a nonstaggered grid by solving two sparse linear systems. The schemes are conservative in all convective fluxes and consistency between the mass variables and pressure is formally maintained.

Numerical experiments are presented to shed light on the inherent differences between the WIMF and SIMF families of schemes. In particular, we demonstrate that the WIMF scheme is able to give an exact resolution of a moving contact discontinuity. The SIMF schemes do not possess the "exact resolution" property of WIMF, however, the ability to take larger time steps can be exploited so that more efficient calculations can be made when accurate resolution of sharp fronts is not essential, e.g. to calculate steady state solutions.

KEY WORDS: Two-phase flow; two-fluid model; hyperbolic system of conservation laws; flux splitting; implicit scheme.

SUBJECT CLASSIFICATION: 76T10, 76N10, 65M12, 35L65.

[1] RF-Rogaland Research, Olav Hanssensvei 15, Stavanger, Norway.
[2] Current address: Centre of Mathematics for Applications, 1053 Blindern, N-0316 Oslo, Norway. E-mails: steinar.evje@rf.no, Tore.Flaatten@rf.no

1. INTRODUCTION

We consider in this paper a classical *two-fluid model* governing two-phase flow of gas and liquid in a pipeline. The model, described in more detail in Section 2, may be written on the following vector form:

$$\partial_t \begin{pmatrix} \rho_g \alpha_g \\ \rho_l \alpha_l \\ \rho_g \alpha_g v_g \\ \rho_l \alpha_l v_l \end{pmatrix} + \partial_x \begin{pmatrix} \rho_g \alpha_g v_g \\ \rho_l \alpha_l v_l \\ \rho_g \alpha_g v_g^2 + \alpha_g p \\ \rho_l \alpha_l v_l^2 + \alpha_l p \end{pmatrix} = \begin{pmatrix} 0 \\ 0 \\ p\partial_x \alpha_g + \tau_g \\ p\partial_x \alpha_l + \tau_l \end{pmatrix} + \begin{pmatrix} 0 \\ 0 \\ Q_g + M_g^D \\ Q_l + M_l^D \end{pmatrix}. \tag{1}$$

Here α_k is the volume fraction of phase k with $\alpha_l + \alpha_g = 1$, ρ_k and v_k denote the density and fluid velocities of phase k, and p is the pressure common to both phases. Moreover, τ_k represents the interfacial forces which contain differential terms (hence, is relevant for the hyperbolicity of the model) and satisfy $\tau_g + \tau_l = 0$. M_k^D represents interfacial drag force with $M_g^D + M_l^D = 0$ whereas Q_k represent source terms due to gravity, friction, etc.

The majority of computer software for such two-fluid simulations are based on implicit time integration, allowing for violation of the CFL criterion

$$\frac{\Delta x}{\Delta t} \geqslant |\lambda_{\max}| \tag{2}$$

where $\lambda_{\max}$ is the largest eigenvalue for the system. Examples include the CATHARE code [1] developed for the nuclear industry, as well as OLGA [2] and PeTra [9] aimed towards the petroleum industry.

Following [7], we classify implicit schemes as follows:

Definition 1 (Weakly implicit). A numerical scheme is said to be **weakly implicit** if it allows stable calculation of solutions under the CFL condition

$$\frac{\Delta x}{\Delta t} \geqslant |\lambda_{\max}^v|, \tag{3}$$

where $\lambda_{\max}^v$ is the largest of the two eigenvalues corresponding to volume fraction waves.

Definition 2 (Strongly implicit). A numerical scheme is said to be **strongly implicit** if it allows stable calculation of solutions under no restriction on the time step related to the wave velocities.

In a previous work [7], we developed a weakly implicit scheme, termed *WIMF-AUSMD*, based on the AUSMD [18] convective fluxes

applied in [6]. A key element in the construction of WIMF-AUSMD was the introduction of the *Mixture Flux* (MF) technique for robust and accurate resolution of both sonic and volume fraction waves.

The purpose of the present work is to elaborate further on the class of MF schemes for the two-fluid model. In particular, we demonstrate how a minor change to the WIMF framework introduced in [7] allows us to obtain a *strongly implicit* scheme in the sense of Definition 2. We proceed as follows:

- First, we construct a fully discrete Weakly Implicit MF scheme, denoted as **WIMF-upwind**, which represents a simplification compared to the WIMF-AUSMD scheme investigated in [7]. The simplification lies in the fact that while WIMF-AUSMD employs an estimate of the sound velocity, **WIMF-upwind** uses no information about the sound velocity.
- Second, we construct a fully discrete Strongly Implicit MF scheme, denoted as **SIMF-upwind**, based on the WIMF-upwind scheme;
- Third, we construct a more robust **SIMF-FVS** scheme, based on the FVS convective fluxes investigated in [6].

Hence this work serves to demonstrate that the MF approach represents a flexible framework which allows us to construct implicit schemes from a broad range of basic convective fluxes.

Numerical simulations are made to highlight the differences and similarities between WIMF-upwind, SIMF-upwind and SIMF-FVS. In particular, we observe the following:

- For time steps dictated by the sonic CFL condition (2) WIMF-upwind and SIMF-upwind give a performance which is similar to an explicit Roe scheme.
- The WIMF-upwind scheme allows *exact* resolution of a moving contact discontinuity. This property closely hangs on the fact that WIMF-type of schemes are stable for time steps dictated by the weak CFL condition (3). Explicit schemes, like the Roe scheme used in this work for comparison purposes, are excluded from possessing this property since the time step must obey the strong CFL condition (2).
- The SIMF-upwind scheme does not possess the "exact resolution property" for a linear contact discontinuity due to the implicit discretization of its numerical mass fluxes. On the other hand, this scheme is *unconditionally* stable for a moving linear contact discontinuity, however at a price of introducing a strong smearing of the contact discontinuity.

- SIMF-FVS is able to handle the transition to one-phase flow in a robust manner. However, SIMF-FVS is more diffusive than SIMF-upwind.

More generally, the results when WIMF and SIMF are explored for different flow cases, indicate that the SIMF scheme allows for an increased time step and improved computational efficiency on a given grid. In particular the SIMF scheme allows for efficient steady state calculations. However, the SIMF is inherently more diffusive than the WIMF on volume fraction waves. This limits the applicability of the SIMF scheme for accurate calculation of slow transients (mass fronts), where a weakly implicit scheme may generally be preferable.

Our paper is organized as follows: In Section 2, the particular two-fluid model we study is presented. In Section 3 we detail the numerical schemes we investigate in this paper. In particular, we develop the WIMF-upwind, SIMF-upwind and SIMF-FVS schemes. In Section 4 the implementation details of the various schemes are discussed; here the band structures of the resulting coefficient matrices are presented.

In Section 5 we highlight an important difference between the WIMF and SIMF classes of schemes, by comparing their formulation for a simple contact discontinuity. Finally, in Section 6 we present numerical simulations. Particularly, we demonstrate that the SIMF scheme introduced in this paper is able to violate the CFL criterion for all waves, justifying its description as a *strongly implicit* scheme. In Section 6.3 we demonstrate that the SIMF-FVS scheme handles the transition to one-phase flow in an efficient and highly robust manner.

2. THE TWO-FLUID MODEL

Throughout this paper we will be concerned with the common two-fluid model formulated by stating separate conservation equations for mass and momentum for the two fluids, which we will denote as a gas (g) and a liquid (l) phase. The model has been studied by several authors [16,3,4,12,6] and will be briefly stated here. We let $\mathbf{U}$ be the vector of conserved variables

$$\mathbf{U} = \begin{bmatrix} \rho_g \alpha_g \\ \rho_l \alpha_l \\ \rho_g \alpha_g v_g \\ \rho_l \alpha_l v_l \end{bmatrix} = \begin{bmatrix} m_g \\ m_l \\ I_g \\ I_l \end{bmatrix}. \tag{4}$$

By using the notation $\Delta p = p - p^i$, where p^i is the interfacial pressure, and $\tau_k = (p^i - p)\partial_x \alpha_k$, we see that the model (1) can be written on the form

- Conservation of mass

$$\frac{\partial}{\partial t}\left(\rho_{\mathrm{g}}\alpha_{\mathrm{g}}\right)+\frac{\partial}{\partial x}\left(\rho_{\mathrm{g}}\alpha_{\mathrm{g}}v_{\mathrm{g}}\right)=0, \tag{5}$$

$$\frac{\partial}{\partial t}\left(\rho_{\mathrm{l}}\alpha_{\mathrm{l}}\right)+\frac{\partial}{\partial x}\left(\rho_{\mathrm{l}}\alpha_{\mathrm{l}}v_{\mathrm{l}}\right)=0, \tag{6}$$

- Conservation of momentum

$$\frac{\partial}{\partial t}\left(\rho_{\mathrm{g}}\alpha_{\mathrm{g}}v_{\mathrm{g}}\right)+\frac{\partial}{\partial x}\left(\rho_{\mathrm{g}}\alpha_{\mathrm{g}}v_{\mathrm{g}}^2\right)+\alpha_{\mathrm{g}}\frac{\partial p}{\partial x}+\Delta p\frac{\partial \alpha_{\mathrm{g}}}{\partial x}=Q_{\mathrm{g}}+M_{\mathrm{g}}^{\mathrm{D}}, \tag{7}$$

$$\frac{\partial}{\partial t}\left(\rho_{\mathrm{l}}\alpha_{\mathrm{l}}v_{\mathrm{l}}\right)+\frac{\partial}{\partial x}\left(\rho_{\mathrm{l}}\alpha_{\mathrm{l}}v_{\mathrm{l}}^2\right)+\alpha_{\mathrm{l}}\frac{\partial p}{\partial x}+\Delta p\frac{\partial \alpha_{\mathrm{l}}}{\partial x}=Q_{\mathrm{l}}+M_{\mathrm{l}}^{\mathrm{D}}. \tag{8}$$

The system is closed by some equation of states (EOS) for the liquid and gas phase. The numerical methods we study in this work allow general expressions for the EOS. However, for the numerical simulations presented in this work we assume the simplified thermodynamic relations

$$\rho_{\mathrm{l}}=\rho_{\mathrm{l},0}+\frac{p-p_0}{a_{\mathrm{l}}^2} \tag{9}$$

and

$$\rho_{\mathrm{g}}=\frac{p}{a_{\mathrm{g}}^2} \tag{10}$$

where

$$p_0=1\ \text{bar}=10^5\ \text{Pa}$$

$$\rho_{\mathrm{l},0}=1000\ \text{kg/m}^3,$$

$$a_{\mathrm{g}}^2=10^5(\text{m/s})^2$$

and

$$a_{\mathrm{l}}=10^3\ \text{m/s}.$$

Moreover, we will treat Q_k as a pure source term, assuming that it does not contain any differential operators. We use the interface pressure correction

$$\Delta p=\sigma\frac{\alpha_{\mathrm{g}}\alpha_{\mathrm{l}}\rho_{\mathrm{g}}\rho_{\mathrm{l}}}{\rho_{\mathrm{g}}\alpha_{\mathrm{l}}+\rho_{\mathrm{l}}\alpha_{\mathrm{g}}}(v_{\mathrm{g}}-v_{\mathrm{l}})^2, \tag{11}$$

where unless otherwise stated we set $\sigma = 1.2$. This choice ensures that the model is a hyperbolic system of conservation laws, see for instance [16, 4]. Another feature of this model is that it possesses an approximate mixture sound velocity c given by

$$c = \sqrt{\frac{\rho_{\mathrm{l}}\alpha_{\mathrm{g}} + \rho_{\mathrm{g}}\alpha_{\mathrm{l}}}{\frac{\partial \rho_{\mathrm{g}}}{\partial p}\rho_{\mathrm{l}}\alpha_{\mathrm{g}} + \frac{\partial \rho_{\mathrm{l}}}{\partial p}\rho_{\mathrm{g}}\alpha_{\mathrm{l}}}}. \tag{12}$$

We refer to [16,6] for more details.

3. NUMERICAL SCHEMES

In this section, we describe the SIMF and WIMF schemes investigated in this paper. The WIMF scheme is elaborately discussed in [7], we here present only the main ideas and the details necessary for implementing the scheme. The SIMF class of schemes differs from WIMF in the level of implicitness of the convective fluxes. This class of schemes is introduced in Section 3.4.

3.1. General Framework

Generally, a numerical approximation of first order temporal accuracy to the system (5)–(8) can be written as follows:

- Gas Mass

$$\frac{m_{\mathrm{g},j}^{n+1} - m_{\mathrm{g},j}^{n}}{\Delta t} + \frac{I_{\mathrm{g},j+1/2}^{*} - I_{\mathrm{g},j-1/2}^{*}}{\Delta x} = 0 \tag{13}$$

- Liquid Mass

$$\frac{m_{\mathrm{l},j}^{n+1} - m_{\mathrm{l},j}^{n}}{\Delta t} + \frac{I_{\mathrm{l},j+1/2}^{*} - I_{\mathrm{l},j-1/2}^{*}}{\Delta x} = 0 \tag{14}$$

- Gas Momentum

$$\frac{I_{\mathrm{g},j}^{n+1} - I_{\mathrm{g},j}^{n}}{\Delta t} + \frac{(Iv)_{\mathrm{g},j+1/2}^{*} - (Iv)_{\mathrm{g},j-1/2}^{*}}{\Delta x} + \alpha_{\mathrm{g},j}^{n}\frac{p_{j+1/2}^{*} - p_{j-1/2}^{*}}{\Delta x} + (\Delta p)_{j}^{n}\frac{\alpha_{\mathrm{g},j+1/2}^{*} - \alpha_{\mathrm{g},j-1/2}^{*}}{\Delta x} = Q_{\mathrm{g},j}^{n} \tag{15}$$

- Liquid Momentum

$$\frac{I_{l,j}^{n+1} - I_{l,j}^{n}}{\Delta t} + \frac{(Iv)_{l,j+1/2}^{*} - (Iv)_{l,j-1/2}^{*}}{\Delta x} + \alpha_{l,j}^{n} \frac{p_{j+1/2}^{*} - p_{j-1/2}^{*}}{\Delta x} + (\Delta p)_{j}^{n} \frac{\alpha_{l,j+1/2}^{*} - \alpha_{l,j-1/2}^{*}}{\Delta x} = Q_{l,j}^{n}. \quad (16)$$

Here we have used the abbreviations

$$m_k = \rho_k \alpha_k \quad (17)$$

and

$$I_k = m_k v_k \quad (18)$$

for phase k. The *-notation indicates that the time level remains to be specified.

The numerical scheme is now determined by the calculation of appropriate cell interface values $(\cdot)_{j+1/2}$ for each time step. The WIMF and SIMF schemes differ only in their treatment of the convective fluxes $I_{j+1/2}$ and $(Iv)_{j+1/2}$. In the following, we will describe the spatial discretization of the remaining terms, defining a common ground for the WIMF and SIMF classes of schemes.

Remark 1. In this paper, we follow [7] and consider only first-order spatial and temporal integration. This is currently the standard for industrial codes [2,9]. However, extensions to higher order accuracy should be explored systematically, with the aim of improving the accuracy of the schemes without hurting the robustness. This could be investigated for instance by following the approach of [10,15].

3.1.1. The Pressure-Momentum Coupling

As noted in [7], an important step towards breaking the CFL criterion for sonic waves is the development of a pressure evolution equation at cell interfaces, and coupling this equation with the mass fluxes.

This gives rise to the following *implicit* algorithm for solving the momentum equations:

- Gas Momentum

$$\frac{I_{\mathrm{g},j}^{n+1}-I_{\mathrm{g},j}^{n}}{\Delta t}+\frac{(Iv)_{\mathrm{g},j+1/2}^{*}-(Iv)_{\mathrm{g},j-1/2}^{*}}{\Delta x}$$
$$+\alpha_{\mathrm{g},j}^{n}\frac{p_{j+1/2}^{n+1}-p_{j-1/2}^{n+1}}{\Delta x}+(\Delta p)_{j}^{n}\frac{\alpha_{\mathrm{g},j+1/2}^{n}-\alpha_{\mathrm{g},j-1/2}^{n}}{\Delta x}=Q_{\mathrm{g},j}^{n} \quad (19)$$

- Liquid Momentum

$$\frac{I_{\mathrm{l},j}^{n+1}-I_{\mathrm{l},j}^{n}}{\Delta t}+\frac{(Iv)_{\mathrm{l},j+1/2}^{*}-(Iv)_{\mathrm{l},j-1/2}^{*}}{\Delta x}$$
$$+\alpha_{\mathrm{l},j}^{n}\frac{p_{j+1/2}^{n+1}-p_{j-1/2}^{n+1}}{\Delta x}+(\Delta p)_{j}^{n}\frac{\alpha_{\mathrm{l},j+1/2}^{n}-\alpha_{\mathrm{l},j-1/2}^{n}}{\Delta x}=Q_{\mathrm{l},j}^{n}. \quad (20)$$

- Pressure Evolution

$$\frac{p_{j+1/2}^{n+1}-\frac{1}{2}(p_{j}^{n}+p_{j+1}^{n})}{\Delta t}=-(\kappa\rho_{\mathrm{l}})_{j+1/2}^{n}\frac{I_{\mathrm{g},j+1}^{n+1}-I_{\mathrm{g},j}^{n+1}}{\Delta x}$$
$$-(\kappa\rho_{\mathrm{g}})_{j+1/2}^{n}\frac{I_{\mathrm{l},j+1}^{n+1}-I_{\mathrm{l},j}^{n+1}}{\Delta x}, \quad (21)$$

where the interface values $\kappa_{j+1/2}^{n}$ and $\rho_{k,j+1/2}^{n}$ are computed from $p_{j+1/2}^{n}$ together with the arithmetic average

$$\alpha_{k,j+1/2}^{n}=\frac{1}{2}(\alpha_{k,j}^{n}+\alpha_{k,j+1}^{n}). \quad (22)$$

Here κ is given by

$$\kappa=\frac{1}{\left(\partial\rho_{\mathrm{g}}/\partial p\right)\rho_{\mathrm{l}}\alpha_{\mathrm{g}}+(\partial\rho_{\mathrm{l}}/\partial p)\,\rho_{\mathrm{g}}\alpha_{\mathrm{l}}}. \quad (23)$$

We refer to [7] for the derivation of the pressure evolution equation. The convective fluxes $(Iv)_{j+1/2}^{*}$ will be defined in Section 3.2.

3.1.2. Source Terms

As may be seen from (19) and (20), the source terms Q_k are discretized explicitly in time. For the test problems investigated in this paper, we consider only gravitational acceleration. Here the explicit integration is sufficient even when the strong CFL criterion (3) is broken.

However, if the source terms are stiff, an implicit discretization may be necessary. This was done in [7].

3.1.3. Interface Pressure Correction Terms

The interface pressure correction term is approximated as follows

$$\left(\Delta p \frac{\partial \alpha_k}{\partial x}\right)_j^n = (\Delta p)_j \frac{\alpha_{k,j+1/2}^n - \alpha_{k,j-1/2}^n}{\Delta x}, \tag{24}$$

where

$$\alpha_{k,j+1/2}^n = \frac{1}{2}(\alpha_{k,j}^n + \alpha_{k,j+1}^n). \tag{25}$$

In other words, we use a simple central, explicit discretization, motivated by the idea that the interface pressure correction is small in magnitude and plays a minor role in the dynamical behaviour of the model [7].

As the numerical examples of this paper demonstrate, the explicit discretization (24) presents no obstacle when it comes to breaking the strong CFL criterion (3).

3.2. Convective Fluxes

By far the most important aspect of the MF methods is the spatial discretization of the convective fluxes. Following [7], we introduce the shorthands

$$F_k = (\rho_k \alpha_k v_k)_{j+1/2} \tag{26}$$

and

$$G_k = (\rho_k \alpha_k v_k^2)_{j+1/2}. \tag{27}$$

We now consider the following basic flux components

- Flux components F^{D} and G^{D} allowing for violation of the sonic CFL criteron (fast waves).
- Flux components F^{A} and G^{A} possessing desirable properties in the resolution of mass transport dynamics (slow waves).

The fluxes F_k and G_k are then constructed as appropriate hybridizations of the underlying "A" and "D" components, with the aim of incorporating properties from both. This motivates the use of the term "mixture flux" (MF) methods.

In the following, we will first describe the general construction of the "A" and "D" flux components (Sections 3.2.1 and 3.2.2) and the appropriate hybridization (Section 3.2.3). Then, in Section 3.3, we define the **upwind** and **FVS** convective splittings. In Section 3.4 we highlight the differences between the SIMF and WIMF classes of schemes.

3.2.1. Flux Components F^D and G^D

The aim of these flux components is to couple the mass calculations $m_{k,j}^{n+1}$ to the pressure calculation $p_{j+1/2}^{n+1}$. Our starting point is the observation that the pressure equation (21) employs the *staggered* Lax–Friedrichs scheme to obtain cell interface values. A projection back to the nonstaggered grid yields *modified Lax–Friedrichs* fluxes [14], which for mass and momentum convection become

$$F_{k,j+1/2}^{\mathrm{D}} = \frac{1}{2}(I_{k,j}^{n+1} + I_{k,j+1}^{n+1}) + \frac{1}{4}\frac{\Delta x}{\Delta t}(m_{k,j}^{n} - m_{k,j+1}^{n}) \tag{28}$$

and

$$G_{k,j+1/2}^{\mathrm{D}} = \frac{1}{2}((Iv)_{k,j}^{n+1} + (Iv)_{k,j+1}^{n+1}) + \frac{1}{4}\frac{\Delta x}{\Delta t}(I_{k,j}^{n} - I_{k,j+1}^{n}). \tag{29}$$

We refer to [7,8] for more details.

Note that we here use *implicit* values for the central flux approximation, and *explicit* values for the numerical viscosity. This is in accordance with the numerical pressure equation (21).

3.2.2. Flux Components F^A and G^A

We write these flux components on the following general form

$$F_{k,j+1/2}^{\mathrm{A}} = V_{k,j}^{+} m_{k,j}^{*} + V_{k,j+1}^{-} m_{k,j+1}^{*} \tag{30}$$

and

$$G_{k,j+1/2}^{\mathrm{A}} = V_{k,j}^{+} I_{k,j}^{*} + V_{k,j+1}^{-} I_{k,j+1}^{*}. \tag{31}$$

Here $V^{\pm}$ are velocity splittings to be defined in Section 3.3, and the *-notation indicates that the time level may be either n or $n+1$. This difference defines the WIMF and SIMF schemes, as described in Section 3.4.

3.2.3. Hybrid Fluxes F_k and G_k

We here consider appropriate hybridizations of the $F^{\mathrm{A,D}}$ and $G^{\mathrm{A,D}}$ fluxes, with the aim that the hybridization should

- reduce to the "D"-component in the resolution of the *pressure* variable (sonic waves).
- reduce to the "A"-component in the resolution of the *volume fraction* variable (material waves).

Based on this motivation, the following hybridizations were obtained in [7, 8] for the convective mass flux F_k:

$$F_{1,j+1/2} = ([\kappa\rho_g\alpha_1\partial_p\rho_1]^n F_1^D + [\kappa\rho_1\alpha_g\partial_p\rho_g]^n F_1^A + [\kappa\rho_1\alpha_1\partial_p\rho_1]^n (F_g^D - F_g^A))_{j+1/2} \tag{32}$$

and

$$F_{g,j+1/2} = ([\kappa\rho_1\alpha_g\partial_p\rho_g]^n F_g^D + [\kappa\rho_g\alpha_1\partial_p\rho_1]^n F_g^A + [\kappa\rho_g\alpha_g\partial_p\rho_g]^n (F_1^D - F_1^A))_{j+1/2}. \tag{33}$$

The coefficient variables at $j+1/2$ are determined from the cell interface pressure $p^n_{j+1/2}$ as well as the relation

$$\alpha^n_{j+1/2} = \frac{1}{2}(\alpha^n_j + \alpha^n_{j+1})$$

which is consistent with the treatment of the coefficients of the pressure evolution equation (21).

Furthermore, based on the assumption that momentum convection affects mainly the material waves (volume fraction variable), we simply use [7, 8]

$$G_{k,j+1/2} = G^A_{k,j+1/2}. \tag{34}$$

Remark 2. In [7], we demonstrated that with an **implicit** "D"-flux and an **explicit** "A"-flux, we could break the CFL-criterion pertaining to the sonic waves. A main aim of this paper is to demonstrate that by treating also the "A"-component of the flux implicitly, we are able to break the CFL criterion for all waves.

3.3. Velocity Splittings

In this section, we describe the two types of convective velocity splittings we apply in this paper; the robust *FVS* splitting investigated in [6], and the less dissipative *upwind* splitting.

3.3.1. FVS

We first define the *cell interface* sound velocity $c_{j+1/2}$

$$c_{j+1/2} = \max(c_j, c_{j+1}), \tag{35}$$

where c is given by (12). Following [6], we now define $V^{\pm}$ as

$$V_{k,j}^{+} = \begin{cases} \frac{1}{4c_{j+1/2}^{n}}(v_{k,j}^{n} + c_{j+1/2}^{n})^2 & \text{if } |v_{k,j}^{n}| < c_{j+1/2}^{n} \\ \frac{1}{2}(v_{k,j} + |v_{k,j}|) & \text{otherwise} \end{cases}, \tag{36}$$

$$V_{k,j+1}^{-} = \begin{cases} -\frac{1}{4c_{j+1/2}^{n}}(v_{k,j+1}^{n} - c_{j+1/2}^{n})^2 & \text{if } |v_{k,j+1}^{n}| < c_{j+1/2}^{n} \\ \frac{1}{2}(v_{k,j+1} - |v_{k,j+1}|) & \text{otherwise} \end{cases}. \tag{37}$$

3.3.2. Upwind

We define the *cell interface* advective velocity $v_{k,j+1/2}$

$$v_{k,j+1/2} = \frac{1}{2}(v_{k,j} + v_{k,j+1}). \tag{38}$$

We now define $V^{\pm}$ as

$$V_{k,j}^{+} = \begin{cases} v_{k,j+1/2}^{n} & \text{if } v_{k,j+1/2}^{n} > 0 \\ 0 & \text{otherwise} \end{cases}, \tag{39}$$

$$V_{k,j+1}^{-} = \begin{cases} v_{k,j+1/2}^{n} & \text{if } v_{k,j+1/2}^{n} < 0 \\ 0 & \text{otherwise} \end{cases}. \tag{40}$$

3.4. WIMF and SIMF Schemes

We are now in a position to precisely define the various schemes we will investigate in this paper. The difference between SIMF and WIMF lies purely in the calculation of the flux componenents F^{A} and G^{A}, where we have

- *WIMF:*

$$F_{k,j+1/2}^{\mathrm{A,WIMF}} = V_{k,j}^{+} m_{k,j}^{n} + V_{k,j+1}^{-} m_{k,j+1}^{n} \tag{41}$$

and

$$G_{k,j+1/2}^{\mathrm{A,WIMF}} = V_{k,j}^{+} I_{k,j}^{n} + V_{k,j+1}^{-} I_{k,j+1}^{n}. \tag{42}$$

- *SIMF:*

$$F^{\mathrm{A,SIMF}}_{k,j+1/2} = V^{+}_{k,j} m^{n+1}_{k,j} + V^{-}_{k,j+1} m^{n+1}_{k,j+1} \tag{43}$$

and

$$G^{\mathrm{A,SIMF}}_{k,j+1/2} = V^{+}_{k,j} I^{n+1}_{k,j} + V^{-}_{k,j+1} I^{n+1}_{k,j+1}. \tag{44}$$

The WIMF-upwind, SIMF-upwind and SIMF-FVS schemes are now defined as follows:

Definition 3 (WIMF-upwind). We will use the term **WIMF-upwind** to denote the numerical algorithm as described in Sections 3.1–3.3, where

- The flux components F^{A} and G^{A} are given by (41) and (42).
- The velocity splittings $V^{\pm}$ are given as described in Section 3.3.2.

Definition 4 (SIMF-upwind). We will use the term **SIMF-upwind** to denote the numerical algorithm as described in Sections 3.1–3.3, where

- The flux components F^{A} and G^{A} are given by (43) and (44).
- The velocity splittings $V^{\pm}$ are given as described in Section 3.3.2.

Definition 5 (SIMF-FVS). We will use the term **SIMF-FVS** to denote the numerical algorithm as described in Sections 3.1–3.3, where

- The flux components F^{A} and G^{A} are given by (43) and (44).
- The velocity splittings $V^{\pm}$ are given as described in Section 3.3.1.

Remark 3. The above WIMF-upwind scheme is simpler than the WIMF schemes considered in [7] in the sense that we do not use any approximate sound velocity. Consequently, no information about the eigenstructure is required.

4. THE MATRIX BAND STRUCTURE

The MF approach, as reflected by the above **WIMF** and **SIMF** schemes, allows for sequential updating of the conservative variables according to the following steps:

(1) The momentum equations (15) and (16) are solved coupled with the pressure equation (21).
(2) The updated mass fluxes $I^{n+1}_{k,j}$ are applied for solving the mass equations.

For **WIMF** the mass equations (13) and (14) with the mixture fluxes (32) and (33) are solved separately and in an explicit manner whereas for **SIMF** the mass equations (13) and (14) with the mixture fluxes (32) and (33) are solved coupled with each other to yield $m_{k,j}^{n+1}$.

The band structure of the resulting linearized systems is described in more detail below.

4.1. The Pressure–Momentum Coupling

The pressure–momentum coupling, as described in Section 3.1.1, gives rise to a linear system that we write on the following form

$$(\mathbf{A}+\mathbf{S})\,\mathbf{x}=\mathbf{b}+\mathbf{w}. \tag{45}$$

We further write each of the matrices $\mathbf{M}=\mathbf{A},\mathbf{S},\mathbf{x},\mathbf{b},\mathbf{w}$ on the following block form

$$\mathbf{M}=\begin{pmatrix} \vdots \\ \mathbf{M}_{j-1} \\ \mathbf{M}_{j} \\ \mathbf{M}_{j+1} \\ \vdots \end{pmatrix}, \tag{46}$$

where in particular

$$\mathbf{x}_j=\begin{pmatrix} I_{\mathrm{g},j} \\ I_{\mathrm{l},j} \\ p_{j+1/2} \end{pmatrix}^{n+1}. \tag{47}$$

Furthermore, $\mathbf{A}$ and $\mathbf{b}$ are common to the WIMF and SIMF schemes. The vector $\mathbf{b}$ is given by

$$\mathbf{b}_j=\begin{pmatrix} I_{\mathrm{g},j}+\Delta t\left(Q_{\mathrm{g},j}-(\Delta p)_j\frac{\alpha_{\mathrm{g},j+1/2}-\alpha_{\mathrm{g},j-1/2}}{\Delta x}\right) \\ I_{\mathrm{l},j}+\Delta t\left(Q_{\mathrm{l},j}-(\Delta p)_j\frac{\alpha_{\mathrm{l},j+1/2}-\alpha_{\mathrm{l},j-1/2}}{\Delta x}\right) \\ \frac{1}{2}(p_j+p_{j+1}) \end{pmatrix}^{n}. \tag{48}$$

Now introducing

$$\delta=\frac{\Delta t}{\Delta x}, \tag{49}$$

the blocks of $\mathbf{A}$ may be written as

$$\mathbf{A}_j = \begin{pmatrix} \ddots & & & & & & \\ \dots & -\alpha_{g,j}\delta & 1 & 0 & \alpha_{g,j}\delta & 0 & 0 & \dots \\ \dots & -\alpha_{l,j}\delta & 0 & 1 & \alpha_{l,j}\delta & 0 & 0 & \dots \\ \dots & 0 & -(\kappa\rho_l)_{j+1/2}\delta & -(\kappa\rho_g)_{j+1/2}\delta & 1 & (\kappa\rho_l)_{j+1/2}\delta & (\kappa\rho_g)_{j+1/2}\delta & \dots \\ & & & & & \ddots & & \end{pmatrix}^n . \tag{50}$$

What remains are the matrices $\mathbf{S}$ and $\mathbf{w}$. These differ in the WIMF and SIMF formulations of the schemes, due to the different treatment of the momentum convection terms.

4.1.1. WIMF

From (42) we obtain

$$\mathbf{S}_j = 0 \tag{51}$$

and

$$\mathbf{w}_j = \begin{pmatrix} -\delta(V^+_{g,j} I_{g,j} + V^-_{g,j+1} I_{g,j+1} - V^+_{g,j-1} I_{g,j-1} - V^-_{g,j} I_{g,j}) \\ -\delta(V^+_{l,j} I_{l,j} + V^-_{l,j+1} I_{l,j+1} - V^+_{l,j-1} I_{l,j-1} - V^-_{l,j} I_{l,j}) \\ 0 \end{pmatrix}^n . \tag{52}$$

4.1.2. SIMF

From (44) we obtain

$$\mathbf{S}_j = \delta \begin{pmatrix} & & \ddots & & & & & & & \\ \dots & -V^+_{g,j-1} & 0 & 0 & V^+_{g,j} - V^-_{g,j} & 0 & 0 & V^-_{g,j+1} & 0 & \dots \\ \dots & 0 & -V^+_{l,j-1} & 0 & 0 & V^+_{l,j} - V^-_{l,j} & 0 & 0 & V^-_{l,j+1} & \dots \\ \dots & 0 & 0 & 0 & 0 & 0 & 0 & 0 & 0 & \dots \\ & & & & & & & \ddots & & \end{pmatrix}^n \tag{53}$$

and

$$\mathbf{w}_j = 0. \tag{54}$$

4.2. The Mass Equations

For the WIMF schemes, the F_k^{A} flux components are evaluated explicitly whereas the F_k^{D} components are known from the previous step as described in Section 4.1. Hence, for the WIMF schemes, the mass equations may be solved directly in an explicit manner by the hybrid fluxes (32) and (33).

For the SIMF schemes, the implicit couplings between the F_k^{A} flux components give rise to a linear system which we write on the form

$$(\mathbf{I}+\delta\mathbf{A})\mathbf{x}=\mathbf{b}, \tag{55}$$

where we reuse the notation of the previous section.

Writing this on the block form (46), we obtain

$$\mathbf{x}_j=\begin{pmatrix}\vdots\\ m_{\mathrm{g,j}}\\ m_{\mathrm{l,j}}\\ \vdots\end{pmatrix}^{n+1} \tag{56}$$

and

$$\mathbf{b}_j=\begin{pmatrix}\vdots\\ m^n_{\mathrm{g,j}}+\delta\left([\kappa\alpha_{\mathrm{g}}\partial_p\rho_{\mathrm{g}}]^n_{j-1/2}[\rho_{\mathrm{l}}^nF_{\mathrm{g}}^{\mathrm{D}}+\rho_{\mathrm{g}}^nF_{\mathrm{l}}^{\mathrm{D}}]_{j-1/2}-[\kappa\alpha_{\mathrm{g}}\partial_p\rho_{\mathrm{g}}]^n_{j+1/2}[\rho_{\mathrm{l}}^nF_{\mathrm{g}}^{\mathrm{D}}+\rho_{\mathrm{g}}^nF_{\mathrm{l}}^{\mathrm{D}}]_{j+1/2}\right)\\ m^n_{\mathrm{l,j}}+\delta\left([\kappa\alpha_{\mathrm{l}}\partial_p\rho_{\mathrm{l}}]^n_{j-1/2}[\rho_{\mathrm{l}}^nF_{\mathrm{g}}^{\mathrm{D}}+\rho_{\mathrm{g}}^nF_{\mathrm{l}}^{\mathrm{D}}]_{j-1/2}-[\kappa\alpha_{\mathrm{l}}\partial_p\rho_{\mathrm{l}}]^n_{j+1/2}[\rho_{\mathrm{l}}^nF_{\mathrm{g}}^{\mathrm{D}}+\rho_{\mathrm{g}}^nF_{\mathrm{l}}^{\mathrm{D}}]_{j+1/2}\right)\\ \vdots\end{pmatrix}, \tag{57}$$

where $F_{\mathrm{g}}^{\mathrm{D}}$ and $F_{\mathrm{l}}^{\mathrm{D}}$ are given by (28).

4.2.1. The Coefficient Matrix **A**

By introducing the shorthands

$$\mu=\kappa\rho_{\mathrm{g}}\alpha_{\mathrm{l}}\partial_p\rho_{\mathrm{l}} \tag{58}$$

$$\nu=\kappa\rho_{\mathrm{l}}\alpha_{\mathrm{l}}\partial_p\rho_{\mathrm{l}} \tag{59}$$

$$\varphi=\kappa\rho_{\mathrm{l}}\alpha_{\mathrm{g}}\partial_p\rho_{\mathrm{g}} \tag{60}$$

$$\psi=\kappa\rho_{\mathrm{g}}\alpha_{\mathrm{g}}\partial_p\rho_{\mathrm{g}} \tag{61}$$

and writing $\mathbf{A}$ as a sum of two components

$$\mathbf{A}=\mathbf{A}_{\mathrm{g}}+\mathbf{A}_{\mathrm{l}}, \tag{62}$$

we find from (32), (33) and (43) that

$$\mathbf{A}_{\mathrm{g},j}=\begin{pmatrix} & \ddots & & & & & \\ \cdots & -\mu_{j-1/2}V^{+}_{\mathrm{g},j-1} & 0 & \mu_{j+1/2}V^{+}_{\mathrm{g},j}-\mu_{j-1/2}V^{-}_{\mathrm{g},j} & 0 & \mu_{j+1/2}V^{-}_{\mathrm{g},j+1} & \cdots \\ \cdots & \nu_{j-1/2}V^{+}_{\mathrm{g},j-1} & 0 & \nu_{j-1/2}V^{-}_{\mathrm{g},j}-\nu_{j+1/2}V^{+}_{\mathrm{g},j} & 0 & -\nu_{j+1/2}V^{-}_{\mathrm{g},j+1} & \cdots \\ & & & & & \ddots & \end{pmatrix}^{n} \tag{63}$$

and

$$\mathbf{A}_{\mathrm{l},j}=\begin{pmatrix} & \ddots & & & & & \\ \cdots & \psi_{j-1/2}V^{+}_{\mathrm{l},j-1} & 0 & \psi_{j-1/2}V^{-}_{\mathrm{l},j}-\psi_{j+1/2}V^{+}_{\mathrm{l},j} & 0 & -\psi_{j+1/2}V^{-}_{\mathrm{l},j+1} & \cdots \\ \cdots & -\varphi_{j-1/2}V^{+}_{\mathrm{l},j-1} & 0 & \varphi_{j+1/2}V^{+}_{\mathrm{l},j}-\varphi_{j-1/2}V^{-}_{\mathrm{l},j} & 0 & \varphi_{j+1/2}V^{-}_{\mathrm{l},j+1} & \cdots \\ & & & & & \ddots & \end{pmatrix}^{n}. \tag{64}$$

The location of the diagonal is indicated by the dots.

5. RESOLUTION OF MOVING OR STATIONARY CONTACT DISCONTINUITY

In this section, we analytically investigate how the different levels of implicitness of WIMF and SIMF affect the resolution of a moving mass front. By this, we aim to illuminate some inherent mechanisms of the WIMF and SIMF schemes.

We consider a contact discontinuity given by

$$\begin{gathered} p_{\mathrm{L}}=p_{\mathrm{R}}=p \\ \alpha_{\mathrm{L}}\neq\alpha_{\mathrm{R}} \\ (v_{\mathrm{g}})_{\mathrm{L}}=(v_{\mathrm{l}})_{\mathrm{L}}=(v_{\mathrm{g}})_{\mathrm{R}}=(v_{\mathrm{l}})_{\mathrm{R}}=v, \end{gathered} \tag{65}$$

for the time period $[t^n, t^{n+1}]$. All pressure terms vanish from the model (5)–(8), and it is seen that the solution to this initial value problem is simply that the discontinuity will propagate with the velocity v. The exact solution of the Riemann problem will then give the numerical mass flux

$$(\rho\alpha v)_{j+1/2}=\frac{1}{2}\rho(\alpha_{\mathrm{L}}+\alpha_{\mathrm{R}})v-\frac{1}{2}\rho(\alpha_{\mathrm{R}}-\alpha_{\mathrm{L}})|v|. \tag{66}$$

We now consider a WIMF scheme where the flux component F_k^{A} reduces to (66) in the resolution of (65), which would be the case for the WIMF-upwind scheme considered here, or the WIMF-AUSMD/V schemes of [7].

Then, as is proved in [7], the WIMF mass fluxes reduce to

$$(\rho_k \alpha_k v_k)_{j+1/2}^{n+1/2} = \rho_k \alpha_{k,j}^n v, \tag{67}$$

where we have assumed that $v \geqslant 0$.

The discrete evolution equation for the mass at cell j is given by

$$\frac{(\rho_k \alpha_k)_j^{n+1} - (\rho_k \alpha_k)_j^n}{\Delta t} = v \frac{(\rho_k \alpha_k)_{j-1}^n - (\rho_k \alpha_k)_j^n}{\Delta x}. \tag{68}$$

Using that ρ_k is constant, this may be simplified to yield the discrete evolution equation for the volume fractions. For simplicity in notation we drop the phase index k and obtain

$$\frac{\alpha_j^{n+1} - \alpha_j^n}{\Delta t} = v \frac{\alpha_{j-1}^n - \alpha_j^n}{\Delta x}. \tag{69}$$

If the contact discontinuity is exactly reproduced within the grid at time $t^n = n\Delta t$, the discrete representation may be expressed as

$$\begin{aligned} \alpha_j^n &= \alpha_{\mathrm{L}} \quad \text{for } j < i, \\ \alpha_j^n &= \alpha_{\mathrm{R}} \quad \text{for } j \geqslant i \end{aligned} \tag{70}$$

for some i. We remember that here $v_{k,j} \equiv v$ and $p_j \equiv p$. From (69) we see that for such an exactly reproduced discontinuity, only the value α_i will change by stepping forward in time from n to $n+1$. We then obtain

$$\frac{\alpha_i^{n+1} - \alpha_{\mathrm{R}}}{\Delta t} = v \frac{\alpha_{\mathrm{L}} - \alpha_{\mathrm{R}}}{\Delta x}. \tag{71}$$

In particular, if $\Delta x / \Delta t = v$ we obtain an interesting result. Then

$$\alpha_i^{n+1} - \alpha_{\mathrm{R}} = \alpha_{\mathrm{L}} - \alpha_{\mathrm{R}} \tag{72}$$

or simply

$$\alpha_i^{n+1} = \alpha_{\mathrm{L}}, \tag{73}$$

whereas

$$\alpha_i^n = \alpha_{\mathrm{R}}. \tag{74}$$

So we conclude that integrating the contact discontinuity (70) using the time step $\Delta x/\Delta t = v$ will shift the location of the discontinuity exactly one grid cell to the right. This is exactly the distance the contact discontinuity will move in one time step, $\Delta x = v\Delta t$. The discrete volume fraction distribution is now given as

$$\begin{aligned} \alpha_j^{n+1} &= \alpha_{\mathrm{L}} \quad \text{for } j < i+1, \\ \alpha_j^{n+1} &= \alpha_{\mathrm{R}} \quad \text{for } j \geqslant i+1, \end{aligned} \tag{75}$$

and by induction

$$\begin{aligned} \alpha_j^{n+m} &= \alpha_{\mathrm{L}} \quad \text{for } j < i+m, \\ \alpha_j^{n+m} &= \alpha_{\mathrm{R}} \quad \text{for } j \geqslant i+m \end{aligned} \tag{76}$$

for all m (within the boundaries of the grid). We may now state the following proposition

Proposition 1. Consider a WIMF type of scheme as described in Section 3.4 with upwind type F_k^{A} flux components. Apply the WIMF scheme to a contact discontinuity moving with the velocity v, as described by (65). If the optimal time step $\Delta x/\Delta t = |v|$ is used, the WIMF scheme will exactly capture the contact discontinuity for all $t^n > t^0$.

Proof. The above discussion proves the Proposition for $v \geqslant 0$. Repeating the steps for $v < 0$ completes the proof. □

Some remarks are now in order.

Remark 4. Notably the proof of Proposition 1 does not rely directly upon the scheme being of the WIMF class. An explicit scheme which correctly reduces to the upwind scheme for the contact discontinuity (65) will also formally satisfy Proposition 1. However, such schemes are unstable under the violation of the sonic CFL criterion implied by the time step $\Delta x/\Delta t = v$. This means that numerical oscillations, however small, will grow exponentially into instabilities.

For the WIMF class of schemes however, the presence of the implicit flux component F_k^{D} as given by (28) will prevent the development of such instabilities.

The ability to exactly capture a contact discontinuity in a stable manner is a very desirable feature unique to the class of WIMF schemes. Numerical evidence of this fact will also be provided in the next section.

Remark 5. Proposition 1 does not apply to the SIMF-upwind scheme as described in Section 3.4. In this case, we may verify that the numerical mass flux becomes

$$(\rho_k \alpha_k v)_{j+1/2}^{n+1} = \rho_k \alpha_{k,j}^{n+1} v \tag{77}$$

for a contact discontinuity of the form (65), and (69) must be replaced by

$$\frac{\alpha_j^{n+1} - \alpha_j^n}{\Delta t} = v \frac{\alpha_{j-1}^{n+1} - \alpha_j^{n+1}}{\Delta x}. \tag{78}$$

Hence SIMF-upwind operates on a contact discontinuity much the same way as an implicit upwind scheme operates on a scalar advection equation. That is, we expect the SIMF class of schemes to be stable, yet diffusive. This issue is explored in the numerical section.

6. NUMERICAL SIMULATIONS

In this section we explore the performance of the various schemes on a simple linear contact discontinuity, the classical "water faucet" benchmark, and a stiff phase separation problem. For comparison we include some results produced by the explicit Roe scheme considered in [6].

6.1. Linear Contact Discontinuity

In the first example we study the performance of WIMF-upwind and SIMF-upwind for a linear contact discontinuity. In particular,

- we want to demonstrate that WIMF-upwind possesses the "exact resolution property" of Proposition 1 and is "weakly implicit" in the sense of Definition 1;
- we want to demonstrate that SIMF-upwind is "strongly implicit" in the sense of Definition 2.

We consider a simple linear contact discontinuity in the volume fraction, where the initial states are given by

$$\mathbf{W}_{\mathrm{L}} = \begin{bmatrix} p \\ \alpha_{\mathrm{l}} \\ v_{\mathrm{g}} \\ v_{\mathrm{l}} \end{bmatrix} = \begin{bmatrix} 10^5\,\mathrm{Pa} \\ 0.75 \\ 10\,\mathrm{m/s} \\ 10\,\mathrm{m/s} \end{bmatrix} \tag{79}$$

and

$$\mathbf{W}_{\mathrm{R}} = \begin{bmatrix} p \\ \alpha_{\mathrm{l}} \\ v_{\mathrm{g}} \\ v_{\mathrm{l}} \end{bmatrix} = \begin{bmatrix} 10^5\,\mathrm{Pa} \\ 0.25 \\ 10\,\mathrm{m/s} \\ 10\,\mathrm{m/s} \end{bmatrix}. \tag{80}$$

We consider a 100 m long pipe and assume that the discontinuity is initially located at $x = 0$. We use a computational grid of 100 cells and simulate a time of $t = 5.0$ s. The discontinuity will then have moved to the center of the pipe, being located at $x = 50$ m.

First, in Fig. 1 we have plotted the solutions produced by the Roe, WIMF-upwind, and SIMF-upwind scheme when the time step corresponding to $\Delta x/\Delta t = 1000$ m/s is applied. This corresponds to the rather small convective CFL

$$\mathrm{CFL}^{\mathrm{conv}} = v\frac{\Delta t}{\Delta x} = 0.01. \tag{81}$$

All three schemes produce upwind type of mass fluxes, and for this time step the solutions are the same, practically speaking.

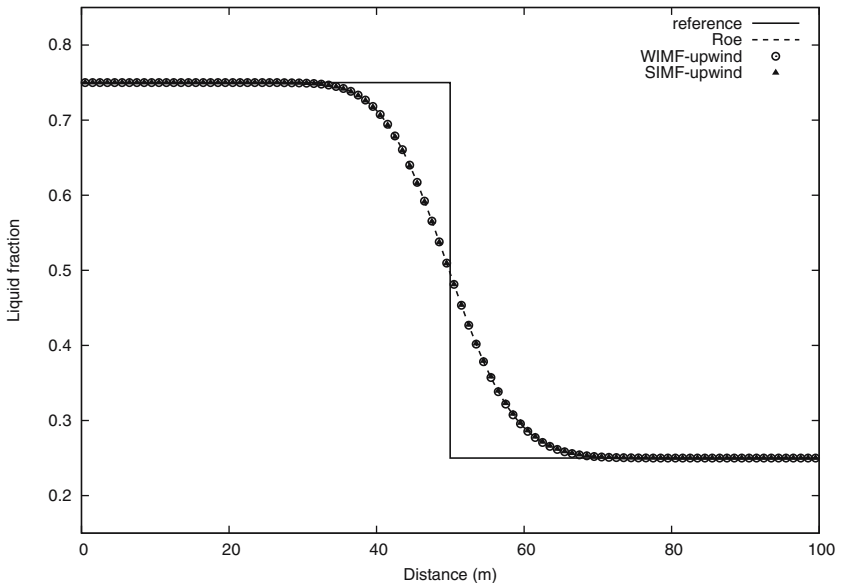

Fig. 1. Linear contact discontinuity, 100 cells, $T = 5.0$ s. Roe, SIMF-upwind, and WIMF-upwind scheme for $\Delta x/\Delta t = 1000$.

Results for different lower values of $\Delta x/\Delta t$ are given in Fig. 2 for the WIMF and SIMF scheme. For these larger values of Δt the Roe scheme becomes unstable since it must obey the sonic CFL condition (2). SIMF-upwind and WIMF-upwind behave similarly for a low time step ($\Delta x/\Delta t = 1000\,\text{m/s}$). However, increasing the time step increases the accuracy for WIMF-upwind but decreases it for SIMF-upwind.

We observe that for the critical time step $\Delta x/\Delta t = v_g = v_l = 10\,\text{m/s}$ (corresponding to a convective CFL of unity), WIMF-upwind captures the discontinuity exactly, as stated by Proposition 1. Increasing the time step beyond this value will make the WIMF-upwind scheme unstable. On the other hand, we may increase the time step beyond $\Delta x/\Delta t = 10\,\text{m/s}$ for SIMF-upwind without inducing instabilities. Once we exceed this critical time step, there is a significant increase in numerical diffusion.

Thus, this example demonstrates that the WIMF-upwind scheme is *weakly implicit* in the sense of Definition 1 whereas the SIMF-upwind scheme is *strongly implicit* in the sense of Definition 2. In addition, we have demonstrated that the WIMF-upwind scheme possesses the 'exact resolution property" of Proposition 1.

6.2. Water Faucet Problem

We consider the classical faucet flow problem of Ransom [13], which has become a standard benchmark [3, 6, 16, 11, 17].

We consider a vertical pipe of length 12 m with the initial uniform state

$$\mathbf{W} = \begin{bmatrix} p \\ \alpha_l \\ v_g \\ v_l \end{bmatrix} = \begin{bmatrix} 10^5\,\text{Pa} \\ 0.8 \\ 0 \\ 10\,\text{m/s} \end{bmatrix}. \tag{82}$$

Gravity is the only source term taken into account, i.e. in the framework of (7) and (8) we have

$$Q_k = g\rho_k\alpha_k, \tag{83}$$

with g being the acceleration of gravity. At the inlet we have the constant conditions $\alpha_l = 0.8$, $v_l = 10\,\text{m/s}$ and $v_g = 0$. At the outlet the pipe is open to the ambient pressure $p = 10^5\,\text{Pa}$. An approximate analytical solution exists for the liquid velocity and volume fraction, see [6,12,17] for details.

In Fig. 3 we compare the SIMF-upwind and the Roe scheme for $T = 0.6\,\text{s}$ on a grid of 120 computational cells. In addition, the effect of reducing the time step corresponding to $\Delta x/\Delta t = 17\,\text{m/s}$ is investigated for the SIMF-upwind and the WIMF-upwind scheme.

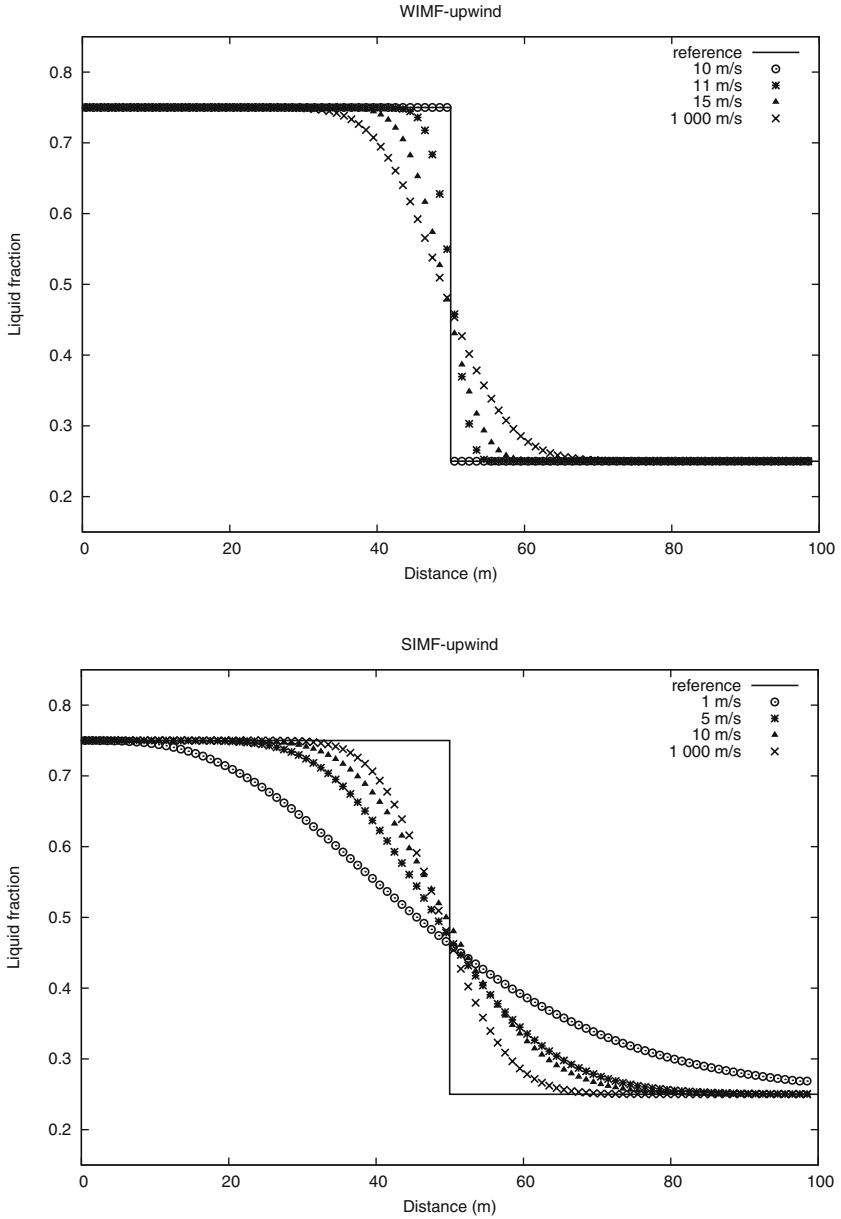

Fig. 2. Linear contact discontinuity, 100 cells. SIMF-upwind vs WIMF-upwind scheme for different values of $\Delta x/\Delta t$. Left: WIMF-upwind. Right: SIMF-upwind.

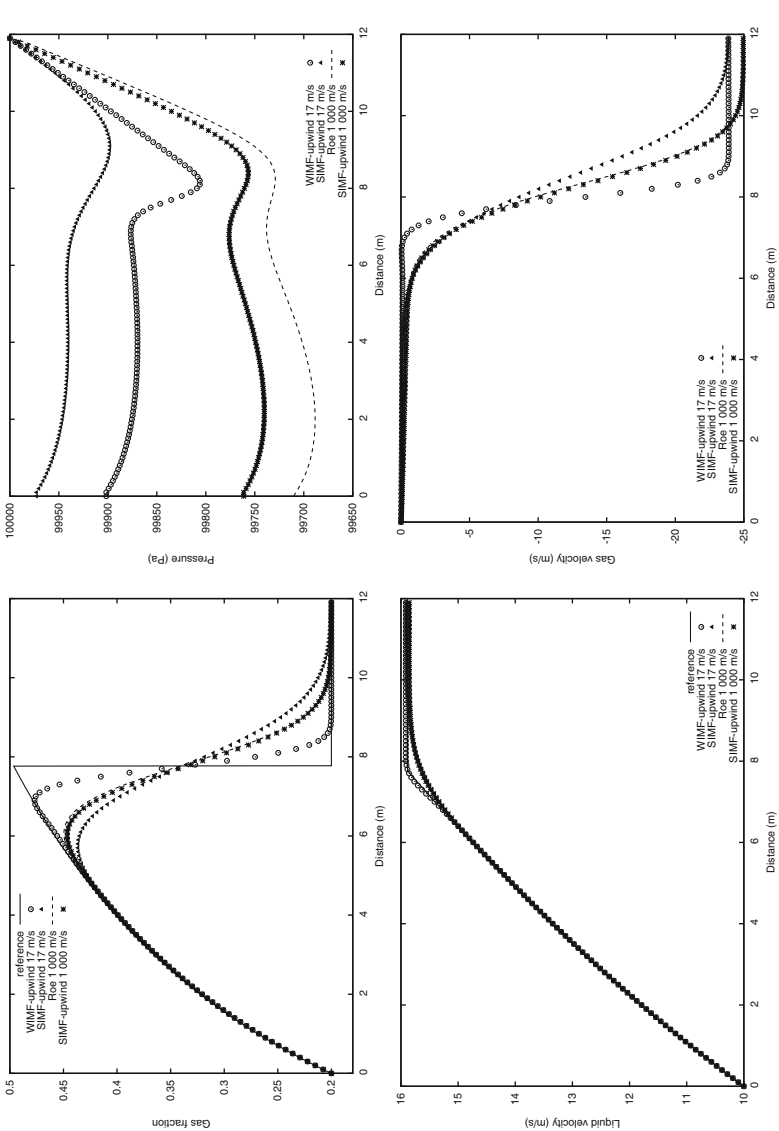

Fig. 3. Water faucet problem, 120 cells, $T = 0.6$ s. SIMF-upwind, WIMF-upwind and Roe scheme. Top left: Gas fraction. Top right: Pressure. Bottom left: Liquid velocity. Bottom right: Gas velocity.

We note that for the small time step corresponding to $\Delta x/\Delta t = 1000\,\text{m/s}$ the SIMF-upwind scheme is virtually indistinguishable from the Roe scheme. Only for the pressure is any difference visible, here the SIMF-upwind scheme is slightly more diffusive.

However, increasing the time step such that $\Delta x/\Delta t = 17\,\text{m/s}$ (approximately the liquid velocity) causes a significant increase in numerical diffusion for the SIMF-upwind scheme, both in pressure and volume fraction. This sharply contrasts the results of the WIMF-upwind scheme, where the lower integration velocity significantly improves the performance of the scheme on the slow waves.

6.2.1. Effect of Increasing the Time Step

We now investigate further how the SIMF and WIMF schemes behave under different time steps. Results after $t = 0.6\,\text{s}$ are given in Fig. 4.

We observe the same picture as for the linear contact discontinuity studied in the previous section. For low time steps, the SIMF-upwind and WIMF-upwind have a similar behaviour. Increasing the time step improves the accuracy of WIMF-upwind but has the opposite effect on the SIMF scheme. Upon breaking the strong (volume fraction) CFL criterion, WIMF-upwind becomes unstable whereas SIMF-upwind merely becomes more diffusive.

Remark 6. These results confirm the picture observed in Section 6.1 and highlight an important difference between the SIMF and WIMF class of schemes. In effect, WIMF-upwind reduces to the upwind explicit flux (67) for a contact discontinuity, whereas SIMF-upwind reduces to the upwind implicit flux (77).

6.2.2. Stationary Solution

We now investigate the performance of the SIMF-upwind scheme for very large time steps, where the volume fraction CFL criterion is strongly violated.

We here use the time step $\Delta t = 5\,\text{s}$, which for the current grid corresponds to a convective CFL of approximately 400. Results after 2, 4 and 7 iterations are given in Fig. 5, where the results are compared to the analytical stationary solutions. We observe that the SIMF-upwind scheme produces qualitatively correct solutions already after 2 iterations. After 7 iterations, the numerical solutions coincide with the analytical reference solutions for liquid velocity and volume fraction.

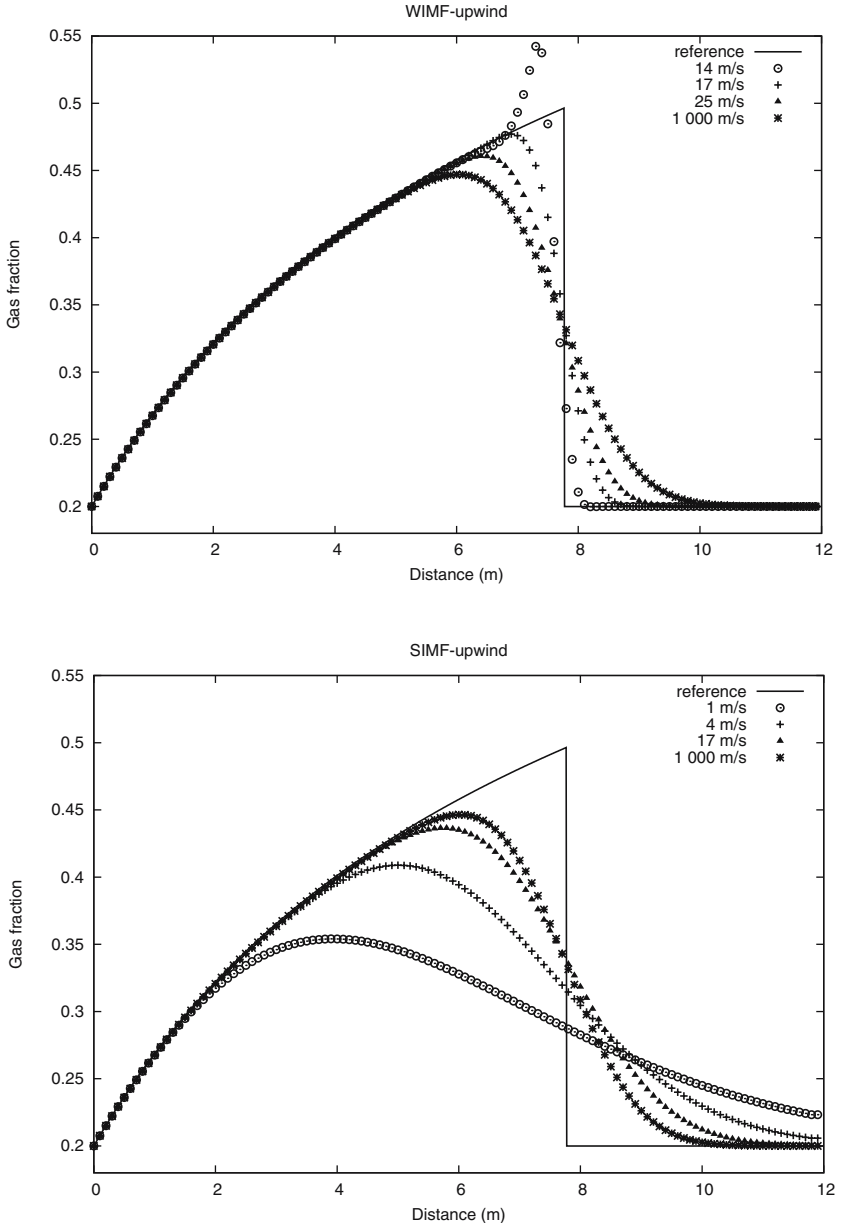

Fig. 4. Water faucet problem, 120 cells. WIMF-upwind vs SIMF-upwind scheme for different values of $\Delta x/\Delta t$. Left: WIMF-upwind. Right: SIMF-upwind.

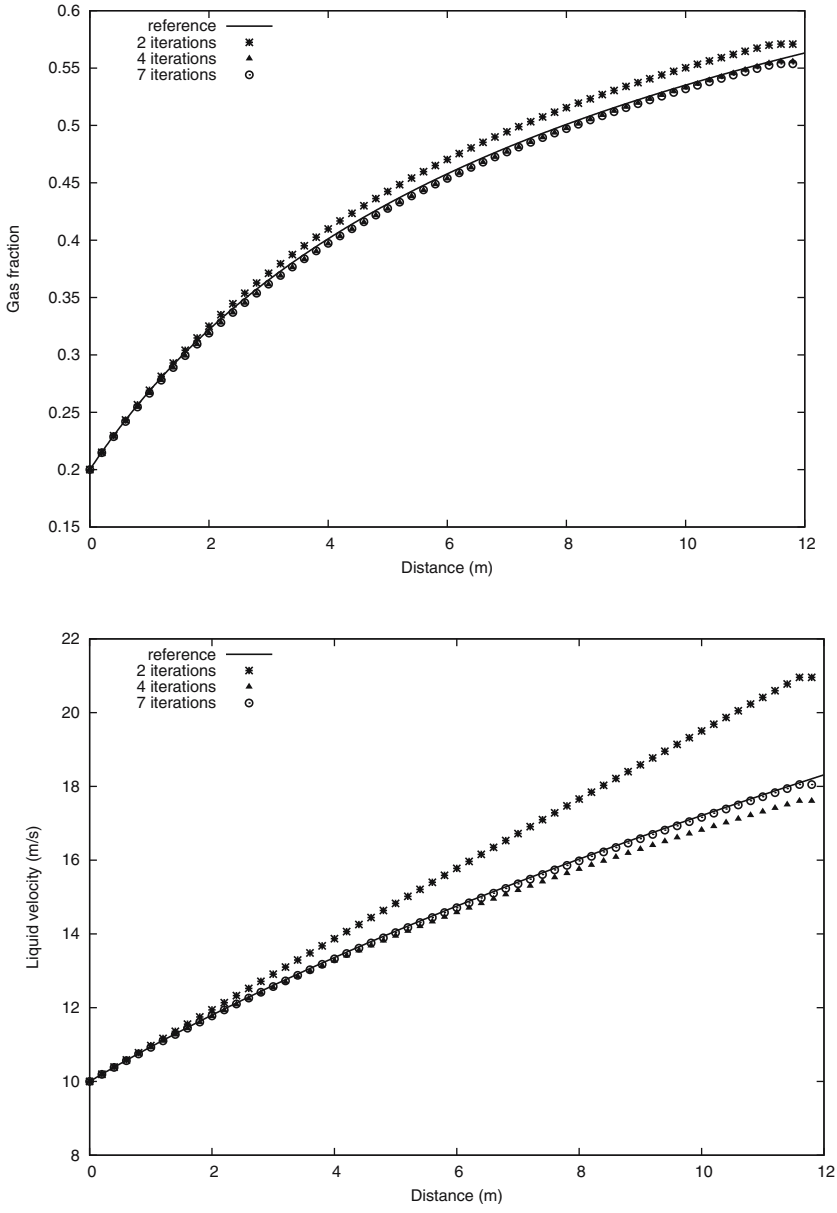

Fig. 5. Water faucet problem, 60 cells, stationary conditions with $\Delta t = 5.0\,\mathrm{s}$. SIMF-upwind vs analytical solution. Left: Gas fraction. Right: Liquid velocity.

6.3. Separation Problem

We follow Coquel et al. [3] and consider a vertical pipe of length 7.5 m, where gravitational acceleration is the only source term taken into account. Initially the pipe is filled with stagnant liquid and gas with a uniform pressure of $p_0 = 10^5$ Pa and a uniform liquid fraction of $\alpha_1 = 0.5$. The pipe is considered to be closed at both ends, i.e. both phasic velocities are forced to be zero at the end points.

An approximate analytical solution may be derived [6] for the evolution of the liquid variables

$$v_1^{\text{ref}}(x,t) = \begin{cases} \sqrt{2gx} & \text{for } x < \frac{1}{2}gt^2 \\ gt & \text{for } \frac{1}{2}gt^2 \leqslant x < L - \frac{1}{2}gt^2 \\ 0 & \text{for } L - \frac{1}{2}gt^2 < x \end{cases} \tag{84}$$

$$\alpha_1^{\text{ref}}(x,t) = \begin{cases} 0 & \text{for } x < \frac{1}{2}gt^2 \\ 0.5 & \text{for } \frac{1}{2}gt^2 \leqslant x < L - \frac{1}{2}gt^2 \\ 1 & \text{for } L - \frac{1}{2}gt^2 < x \end{cases} \tag{85}$$

When the phases are fully separated, we expect the pressure distribution to be fully hydrostatic, approximately given by

$$p^{\text{ref}}(x,t) = \begin{cases} p_0 & \text{for } x < L/2 \\ p_0 + \rho_1 g\,(x - L/2) & \text{for } x \geqslant L/2. \end{cases} \tag{86}$$

6.3.1. Numerical Results for the Stationary State

Using a grid of 1000 cells and the time step corresponding to $\Delta x/\Delta t = 60$ m/s, results for the SIMF-FVS scheme are plotted in Fig. 6 at the time $T = 3.0$ s. The calculation has now settled to the stationary state, although artificial velocity profiles remain due to numerical diffusion.

The scheme handles well the transition to one-phase flow for this difficult test case. The lack of friction terms causes the gas velocity to be large as the gas phase is disappearing, which causes the pressure distribution to deviate slightly from the expected hydrostatic distribution.

Remark 7. The SIMF-upwind and WIMF-upwind schemes do not possess a sufficiently strong numerical dissipation mechanism to handle the transition to one-phase flow in a satisfactory manner. This may be remedied by taking advantage of the excellent stability properties of the FVS flux splitting in one-phase regions, following the approach of [6, 7].

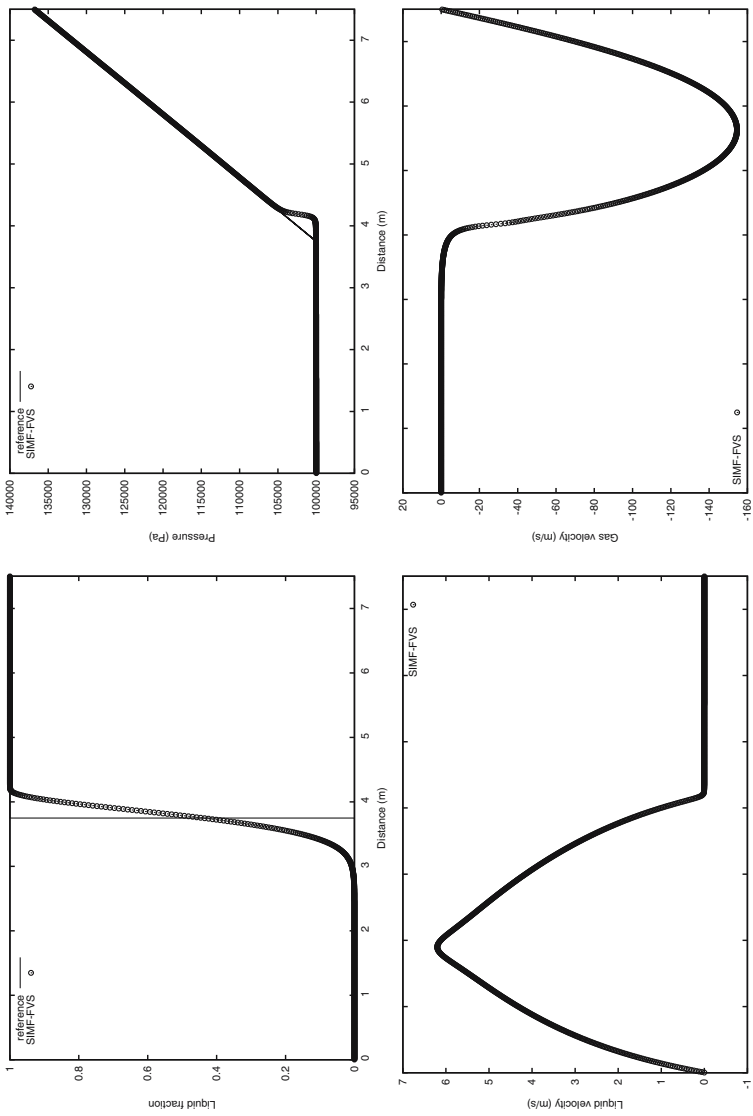

Fig. 6. Separation problem, 1000 cells. SIMF-FVS scheme at $T = 3.0$ s. Top left: Liquid fraction. Top right: Pressure. Bottom left: Liquid velocity. Bottom right: Gas velocity.

Remark 8. An eigenvalue analysis [6] demonstrates that the volume fraction wave velocities are roughly given by

$$\lambda^{\mathrm{v}} = \frac{\rho_{\mathrm{g}}\alpha_{\mathrm{l}} v_{\mathrm{g}} + \rho_{\mathrm{l}}\alpha_{\mathrm{g}} v_{\mathrm{l}}}{\rho_{\mathrm{g}}\alpha_{\mathrm{l}} + \rho_{\mathrm{l}}\alpha_{\mathrm{g}}} \pm \sqrt{\frac{\Delta p(\rho_{\mathrm{g}}\alpha_{\mathrm{l}} + \rho_{\mathrm{l}}\alpha_{\mathrm{g}}) - \rho_{\mathrm{l}}\rho_{\mathrm{g}}\alpha_{\mathrm{l}}\alpha_{\mathrm{g}}(v_{\mathrm{g}} - v_{\mathrm{l}})^2}{(\rho_{\mathrm{g}}\alpha_{\mathrm{l}} + \rho_{\mathrm{l}}\alpha_{\mathrm{g}})^2}}. \quad (87)$$

For this particular problem we see that these are approximately given by the gas velocity as the gas phase is disappearing. As the maximum gas velocity here becomes higher than the integration parameter $\Delta x/\Delta t$, we see that

$$\mathrm{CFL}^{\mathrm{conv}} = \max|\lambda^{\mathrm{v}}|\frac{\Delta t}{\Delta x} > \frac{\Delta x}{\Delta t}\frac{\Delta t}{\Delta x} = 1.$$

Thus, we conclude that the SIMF-FVS scheme is able to violate the CFL criterion for both sonic and volume fraction waves for this problem. In particular, SIMF-FVS allows a choice of time step an order of magnitude larger than the choice used for the WIMF-AUSMDV* scheme in [7].

6.3.2. Convergence Properties of SIMF-FVS

In Fig. 7 we investigate the convergence of the SIMF-FVS scheme as the grid is refined. A plot of the liquid fraction is made at the time $T = 0.6$ s. The SIMF-FVS scheme approximates the expected solution in a monotone way. The convergence rate is given in Table 1, where the error is measured by the 1-norm

$$||E|| = \sum_j \Delta x|\alpha_{\mathrm{l},j} - \alpha_{\mathrm{l},j}^{\mathrm{ref}}|. \quad (88)$$

The order of convergence s is obtained through

$$s_n = \frac{\ln(||E||_n/||E||_{n-1})}{\ln(\Delta x_n/\Delta x_{n-1})}. \quad (89)$$

Although the SIMF-FVS scheme is formally of first order, the convergence rate s is significantly less; this is due to the discontinuities in the solution.

7. SUMMARY

We have constructed a framework termed *Strongly Implicit Mixture Flux* (SIMF) which allows us to construct CFL-violating numerical schemes for a standard two-fluid model. Within this framework we have constructed natural extensions of the schemes investigated by Evje et al [5, 6, 7], resulting in the SIMF-upwind and SIMF-FVS schemes.

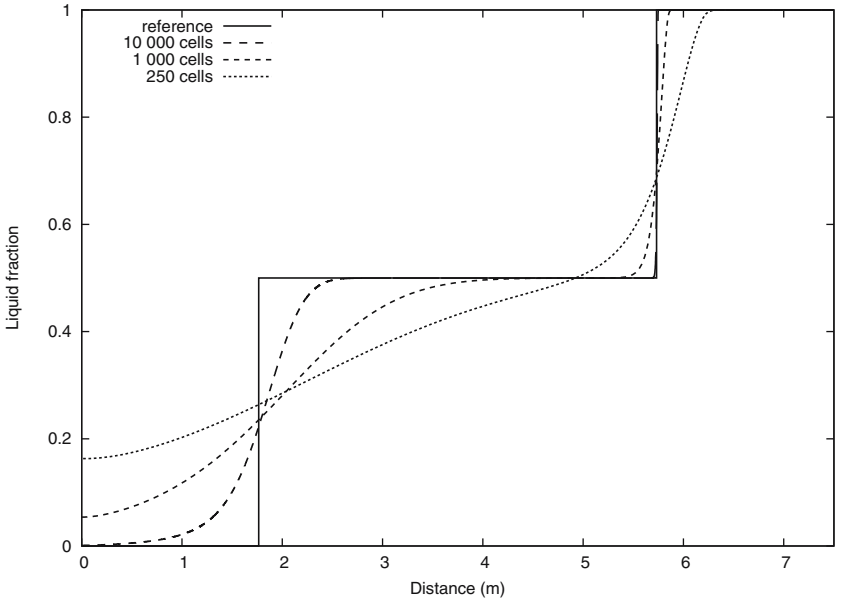

Fig. 7. Separation problem, $T = 0.6$ s. Convergence properties of the SIMF-FVS scheme.

Table I. Separation Problem, $T = 0.6$ s. Convergence Rates for the SIMF-FVS Scheme

n	cells	$\|\|E\|\|_n$	s_n
1	100	1.158	
2	250	0.8139	0.3849
3	1000	0.4473	0.4318
4	10000	0.1497	0.4754

We have demonstrated that the SIMF-upwind scheme possesses accuracy and stability properties comparable to the Roe scheme for small time steps. On breaking the sonic CFL criterion, the SIMF-upwind scheme becomes less accurate than its weakly implicit variant WIMF-upwind in the resolution of volume fraction waves. As opposed to the SIMF-upwind scheme, the WIMF scheme is in fact able to capture a moving contact discontinuity *exactly*.

On the other hand, the SIMF family of schemes, in particular SIMF-FVS, possesses excellent robustness properties. Hence they are well suited for steady state solvers or for cases where a computationally cheap qualitative description of the transient is desired.

ACKNOWLEDGEMENTS

The second author thanks the Research Council of Norway for financial support through the "Petronics" programme. The authors also thank the referees and editor for their valuable remarks which led to a substantial improvement of the first version of this paper.

REFERENCES

1. Barre, F. *et al*. (1990). The cathare code strategy and assessment. *Nucl. Eng. Des*. **124**, 257–284.
2. Bendiksen, K. H., Malnes, D., Moe, R., and Nuland, S. (1991). The dynamic two-fluid model OLGA: Theory and application. *SPE Prod. Eng*. **6**, 171–180.
3. Coquel, F., El Amine, K., Godlewski, E., Perthame, B., and Rascle, P. (1997). A numerical method using upwind schemes for the resolution of two-phase flows. *J. Comput. Phys*. **136**, 272–288.
4. Cortes, J., Debussche, A., and Toumi, I. (1998). A density perturbation method to study the eigenstructure of two-phase flow equation systems. *J. Comput. Phys*. **147**, 463–484.
5. Evje, S., and Fjelde, K. K. (2003). On a rough ausm scheme for a one-dimensional two-phase flow model. *Comput. Fluids* **32**, 1497–1530.
6. Evje, S., and Flåtten, T. (2003). Hybrid flux-splitting schemes for a common two-fluid model. *J. Comput. Phys*. **192**, 175–210.
7. Evje, S., and Flåtten, T. (2005). Weakly implicit numerical schemes for a two-fluid model. *SIAM J. Sci. Comput.* **26**, 1449–1484.
8. Evje, S., and Flåtten, T. (2005). Hybrid central-upwind schemes for numerical resolution of two-phase flows. *ESAIM-Math. Model. Num.* **39**, 253–274.
9. Larsen, M., Hustvedt, E., Hedne, P., and Straume, T. Petra: A novel computer code for simulation of slug flow, in *SPE Annual Technical Conference and Exhibition*, SPE 38841, p. 1–12, October 1997.
10. Lorentzen, R. J., and Fjelde, K. K. (2005). Use of slopelimiter techniques in traditional numerical methods for multi-phase flow in pipelines and wells. *Int. J. Numer. Meth. Fluids* **48**, 723–745.
11. Niu, Y.-Y. (2001). Advection upwinding splitting method to solve a compressible two-fluid model. *Int. J. Numer. Meth. Fluids* **36**, 351–371.
12. Paillère, H., Corre, C., and Cascales, J. R. G (2003). On the extension of the AUSM+ scheme to compressible two-fluid models. *Comput. Fluids* **32**, 891–916.
13. Ransom, V. H. (1987). Numerical bencmark tests, *Multiphase Sci. Tech.* **3**, 465–473.
14. Tadmor, E. (1984). Numerical viscosity and the entropy condition for conservative difference schemes. *Math. Comput.* **43**, 369–381.
15. Toumi, I., and Caruge, D. (1998). An Implicit Second-Order Numerical Method for Three-Dimensional Two-Phase Flow Calculations. *Nucl. Sci. Eng.* **130**, 213–225.
16. Toumi, I., and Kumbaro, A. (1996). An approximate linearized riemann solver for a two-fluid model. *J. Comput. Phys.* **124**, 286–300.
17. Trapp, J. A., and Riemke, R. A. (1986). A nearly-implicit hydrodynamic numerical scheme for two-phase flows. *J. Comput. Phys.* **66**, 62–82.
18. Wada, Y., and Liou, M.-S. (1997). An accurate and robust flux splitting scheme for shock and contact discontinuities. *SIAM J. Sci. Comput*. **18**, 633–657.